Spatial Localization of Excitons and Charge Carriers in Hybrid Perovskite Thin Films

*Mary Jane Simpson,[†] Benjamin Doughty,[†] Bin Yang,[‡] Kai Xiao,[‡] Ying-Zhong Ma†**

[†]Chemical Sciences Division, Oak Ridge National Laboratory, Oak Ridge, Tennessee, 37831

[‡]Center for Nanophase Materials Sciences, Oak Ridge National Laboratory, Oak Ridge, Tennessee, 37831

*Corresponding author: may1@ornl.gov

ABSTRACT: The fundamental photophysics underlying the remarkably high power conversion efficiency of organic-inorganic hybrid perovskite-based solar cells has been increasingly studied using complementary spectroscopic techniques. However, the spatially heterogeneous polycrystalline morphology of the photoactive layers owing to the presence of distinct crystalline grains has been generally neglected in optical measurements and therefore the reported results are typically averaged over hundreds or even thousands of such grains. Here, we apply femtosecond transient absorption microscopy to spatially and temporally probe ultrafast electronic excited-state dynamics in pristine methylammonium lead tri-iodide ($CH_3NH_3PbI_3$) thin films and composite structures. We found that the electronic excited-state relaxation kinetics are extremely sensitive to the sample location probed, which was manifested by position-dependent decay timescales and transient signals. Analysis of transient absorption kinetics acquired at distinct spatial positions enabled us to identify contributions of excitons and free charge carriers.

Table of Contents Graphic

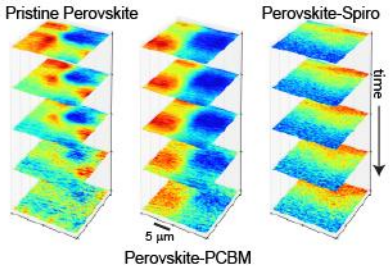

KEYWORDS: Transient absorption microscopy (TAM), ultrafast electronic excited-state spectroscopy, Auger recombination, exciton-exciton annihilation, time-resolved optical imaging, perovskite

The remarkably high power conversion efficiencies achieved with solution-processed organometallic halide perovskite-based solar cells in recent years has stimulated increasingly intensive efforts to understand the fundamental photophysics underlying their impressive performance[1-3]. Detailed experimental studies have been reported by several laboratories employing complementary spectroscopic techniques, including linear absorption[4], steady-state and time-resolved photoluminescence (PL)[5-10], femtosecond transient absorption[8, 9, 11-15], THz spectroscopies[16-18], and microwave conductivity measurements[16, 19]. However, fundamental questions such as the nature of photoexcited species being either neutral excitons, free charge carriers or their coexistence have been debated. This lack of understanding further leads to a controversial assignment for the origin of the observed PL to either exciton relaxation[5, 6, 10] or to the radiative recombination of charge carriers[8]. Even more problematic is that most of the spectroscopic studies did not take into account the spatially heterogeneous polycrystalline morphology of these perovskite-based materials, that arise from the presence of crystalline grains with remarkably different size, shape, and possibly distinct level of defects[2, 10, 20, 21]. Because these spectroscopic measurements have been performed almost exclusively at an ensemble level, which typically probe several tens to hundreds of micrometers of material, the experimental results obtained represent an *average* description of the optical properties for many distinct grains. Consequently, these results cannot distinguish the detailed electronic excited-state dynamics associated with different crystalline grains or, equivalently, distinct spatial locations of these thin films. An unambiguous understanding of the electronic excited-state processes and physical mechanisms requires an ultrafast spectroscopic technique that is capable of not only high temporal resolution, but also sufficient spatial resolution in order to selectively probe the

electronic excited-state dynamics associated with micrometer-sized crystalline grains or thin film areas.

Here, we report an experimental study of spatially resolved ultrafast electronic excited-state dynamics in pristine and composite perovskite thin films using femtosecond transient absorption microscopy (TAM)[22]. The most striking finding of our measurements is that the transient absorption (TA) kinetics extracted from the images are extremely sensitive to the spatial positions probed in the perovskite samples, which is manifested by distinct decay signatures and TA signal signs, i.e., signals are composed of induced transmission (positive) and induced absorption (negative) characteristics that evolve on distinct timescales. Acquisition of TA images at variable time delays allows for the identification of distinct spatial features that are significantly larger in size than the typical ~1-4 μm grains observed for samples prepared on planar substrates using post-annealing processing in this and previous work[2, 10, 20, 21]. These results suggest that the excited state dynamics are not necessarily heterogeneous on a grain-to-grain scale, but rather are heterogeneous over a larger length scale. Analysis of the kinetic data extracted from distinct spatial locations further allows us to identify the coexistence of both neutral excitons and free charge carriers that are formed at particular locations in the thin films. The results underscore the need to resolve electronic excited-state dynamics of complex materials in both space and time in order to understand the fundamental photophysics at the heart of light harvesting and emitting technologies.

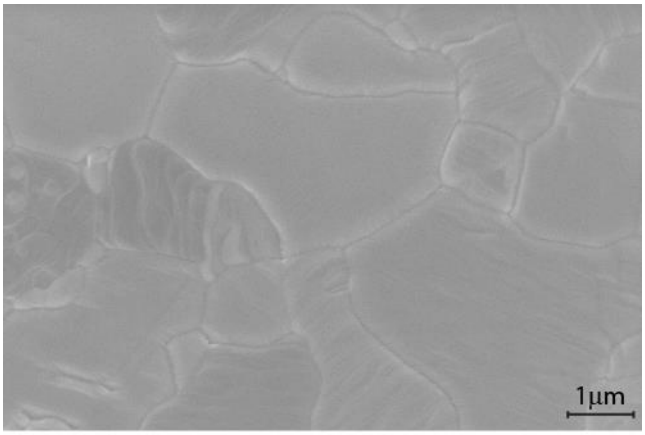

Figure 1. SEM image of pristine $CH_3NH_3PbI_3$ film.

Figure 1 shows the surface morphological image of a pristine $CH_3NH_3PbI_3$ thin film acquired using a scanning electron microscope (SEM, Zeiss Merlin SEM) with a gun voltage of 5 KV, where distinct grains with typical size on the order of 1-4 μm is clearly evident. Representative TA images collected for the pristine $CH_3NH_3PbI_3$, $CH_3NH_3PbI_3$/ PCBM and $CH_3NH_3PbI_3$/Spiro-OMeTAD samples at five delay times are shown in Fig. 2. From the images collected from the first two samples, one can immediately identify several striking features. First, the signs of the observed TA signals depend strongly on the spatial position probed in the individual samples, and display amplitudes with signs that vary from positive-signed photo-induced transmission to negative-signed photo-induced absorption. Signals with a positive sign arise from more probe light reaching the detector as compared to the case when the pump pulse is absent; such signals correspond to stimulated emission and ground state bleaching. Negative signals correspond to excited state absorption, where the probe photon induces an electronic transition from the initially prepared photoexcited state created by the pump pulse to a higher-lying excited state(s). Second, the observed spatial features evolve temporally on distinct timescales, which can be seen

by comparing the images collected at different delay times. Third, the observed spatial features are significantly larger than the typical grain sizes, which are on the order of 1-4 μm for the samples prepared on planar substrates using post-annealing processing as shown in Fig. 1 and also refs. 2, 10, 20, 21. In fact, the observed feature size is comparable to that seen in recently reported one- and two-photon fluorescence imaging studies[23], implying that the excitation distribution occurs on a larger length scale than the spatial heterogeneity. Besides these general similarities, the TA images acquired for the $CH_3NH_3PbI_3$/ PCBM sample also exhibit noticeable differences from the corresponding images obtained from the pristine $CH_3NH_3PbI_3$ sample, manifesting in relatively larger features and less dramatic variations with time. In striking contrast, the TA images measured from the $CH_3NH_3PbI_3$/Spiro-OMeTAD sample are substantially different from the previous two samples, in that larger spatial features are observed and only signals with the same sign are found across the entire image at any given delay time. The general observations described above are consistent from experiment-to-experiment at different locations of the same type samples, which were performed over several separate experimental runs to ensure reproducibility and consistency of the sample preparation and TAM measurements.

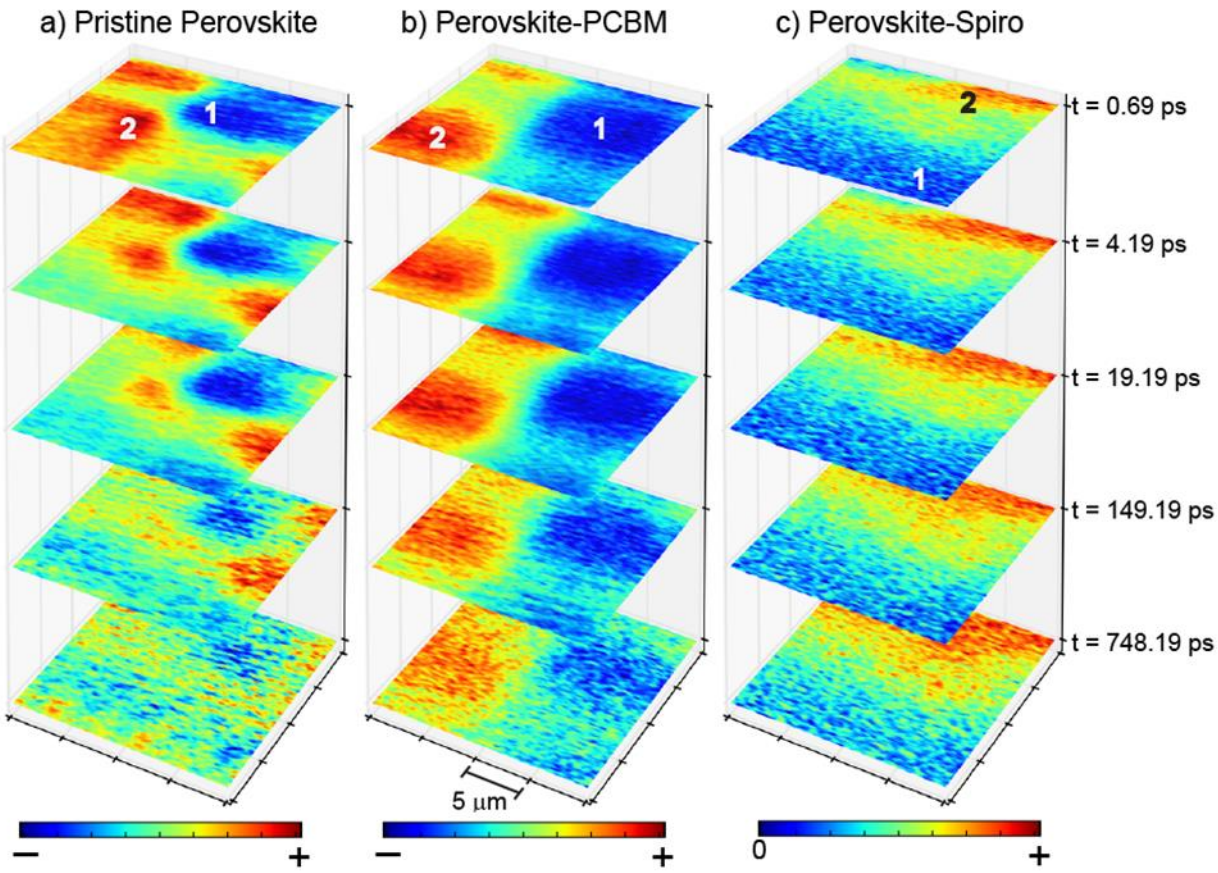

Figure 2. TAM images acquired for the same area of the pristine $CH_3NH_3PbI_3$ (a), $CH_3NH_3PbI_3$/PCBM (b), and $CH_3NH_3PbI_3$/ Spiro-OMeTAD (c) samples at five different delay times as indicated. Scale bars are 5 µm, and the color scales at the bottom depict the variation of TAM signal sign and amplitude for the images shown. Amplitudes of each image are scaled to emphasize spatial features; absolute intensities for each image are given in Supplementary Table 2.

The remarkable dependence of the observed TA signals on the sample spatial location probed can be more clearly seen by directly comparing the kinetic traces obtained by integrating over smaller 1.6 µm × 1.6 µm areas at selected positions of the TA images shown in Fig. 2 and plotting those signals as a function of the delay time between the pump and probe pulses. The

size of these areas was chosen to achieve a good signal-to-noise ratio in the extracted transients, while being small enough to avoid averaging between clearly spatially heterogeneous locations of the TA images. There were no significant differences in the results by making the regions larger or smaller as long as the signal integration area is within a chosen spatial feature. Figures 3a, b and c show the kinetics obtained from two different positions of the TA images acquired from the pristine $CH_3NH_3PbI_3$, $CH_3NH_3PbI_3$/PCBM, and $CH_3NH_3PbI_3$/Spiro-OMeTAD samples, respectively. The positions where these kinetic profiles were obtained are indicated on the corresponding TA images shown in Fig. 2. For comparison, the scaled kinetic traces obtained by integrating an entire 20 μm × 20 μm image area are also shown for all three samples. For both the pristine $CH_3NH_3PbI_3$ and $CH_3NH_3PbI_3$/PCBM samples, the kinetic traces are strongly dependent on the spatial position that is interrogated, which is manifested by not only a change of TA signal sign (from induced transmission to induced absorption), but also by clearly different decay timescales and associated amplitudes. Even though the three kinetic traces obtained for the $CH_3NH_3PbI_3$/Spiro-OMeTAD sample are generally similar, showing at all positions a pronounced induced absorption signal that rapidly changes to an induced transmission signal, the subsequent decays are again dependent on the spatial location probed in the sample. For all three samples, the most significant observation is that the TA kinetics obtained by integrating the entire 20 μm × 20 μm image area are substantially different from either of the kinetic traces obtained by integrating a smaller area at the two selected spatial positions.

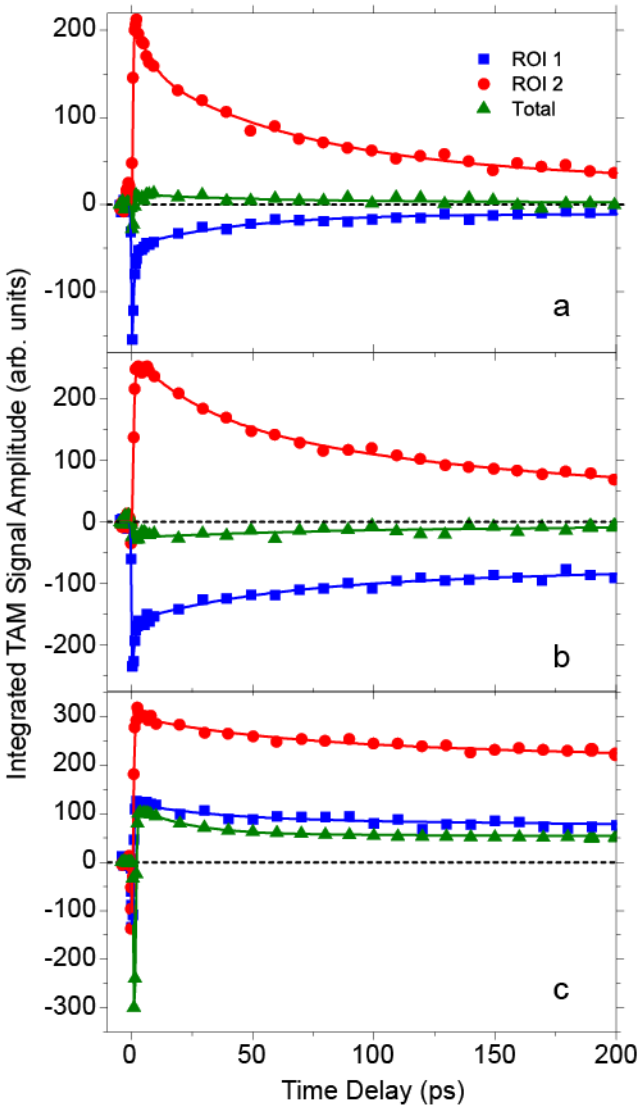

Figure 3. TA kinetics at two different locations of the TAM images acquired from pristine $CH_3NH_3PbI_3$ (a), $CH_3NH_3PbI_3$/PCBM (b), and $CH_3NH_3PbI_3$/ Spiro-OMeTAD (c) samples. The precise locations are indicated in the corresponding TAM images shown in Figure 2. These kinetic traces were obtained by integrating a 1.6 μm × 1.6 μm image area, and the kinetics obtained by integrating the entire 20 μm × 20 μm image area are also shown (dark green triangles). The solid lines are the results of deconvolution fitting as described in the Supplementary Methods, and the dash lines show the baseline for the each panel. Note that TA

kinetics collected over the entire range of delay times (850 ps) are shown in Supplementary Figure 2.

A similar spatial-dependence of TA kinetics was observed by Katayama *et al.* in their TA imaging measurements of a $CH_3NH_3PbI_3$ perovskite-based solar cell fabricated on a mesoporous TiO_2 layer under lower pump and probe intensities[24]. Although the signal-to-noise of their reported results is poorer than ours, a variation of the TA signal sign at different sample position was clearly evident. As our probe pulse centered at 800 nm is very close to the zero-crossing point of the TA spectra measured from the same kind of perovskite films,[14, 25] a clear shift of the linear absorption spectra from one grain to another could give rise to position-dependent TA signal sign. However, the broad probe spectrum (~20 nm, full-width at half maximum) and negligible absorption edge shift for the small grains present in our films[21, 24] make this very unlikely. Thus, these offer strong support that our observed change in the TA signal sign represents an intrinsic property of these pristine and composite perovskite samples rather than an unwanted nonlinear effect, as will be discussed in more detail below. Use of planar substrates in our current study enabled us to address the fundamental photophysics without a potential complication arising from a spatial confinement effect owing to perovskite infiltrated into a mesoporous substrate. Additionally, the pulse intensities used here are higher, which enable us to acquire high quality images and use them to distinguish contributing photoexcited species through analysis of nonlinear excitation phenomena, as will be discussed in the following sections. All together, these observations unambiguously demonstrate a spatial dependence of the electronic excited-state dynamics in the pristine and composite perovskite thin films. Given the polycrystalline morphology due to the presence of crystalline grains with variable size and shape as shown in Fig. 1, as well as possibly distinct level of defects from one position to

another, it is perhaps not surprising that the TA kinetics are so sensitive to the spatial position within these materials. Furthermore, as ensemble TA measurements integrate the entire spatial overlapping region of the pump and probe beam spots, which have typical diameters ranging from tens to hundreds of micrometers, the results will describe an average over hundreds or thousands of individual crystalline grains. It can therefore be fairly difficult to capture the electronic excited-state dynamics associated with well-defined crystalline grains of micrometer size using more commonly employed ensemble measurements. Unless the sampling area is sufficient large, the data collected using ensemble measurements might even vary with the sample position or/and the changes in the spot size of the pump and probe beams. This further highlights the critical need for simultaneous high spatial and temporal resolution in order to unambiguously identify the nature of photoexcitations and reveal their intrinsic ultrafast excited-state dynamics and underlying physical mechanisms in such structurally heterogeneous systems.

Turning attention back to the kinetic data shown in Fig. 3, one can see that the presence of either PCBM or Spiro-OMeTAD leads to noticeably slower decays than what was observed from pristine $CH_3NH_3PbI_3$ samples. This is clearly inconsistent with previous ensemble TA measurements using lower pump intensities[9]. However, given the higher pump and probe intensities used in our TAM measurements we expect that nonlinear electronic excited-state phenomena, including exciton-exciton annihilation[26] and Auger recombination of charge carriers[27, 28], can play a significant role in the relaxation processes. In this case, the presence of either PCBM or Spiro-OMeTAD will facilitate exciton dissociation, leading to a decreased exciton population and in turn the contribution from these nonlinear processes will become less prominent in the kinetics. Although the exciton diffusion constant is only 0.01 cm^2s^{-1} [25], the

incident laser beams strike the hole or electron transport layer prior to reaching the perovskite films (see Supplementary Fig. 1 for our sample geometries) and therefore the excitons generated in the interfacial region can be quenched very rapidly. Consequently, the TA kinetics with hole or electron transport layers should exhibit *slower* decays than those observed from pristine $CH_3NH_3PbI_3$ samples, as was observed here. It should be emphasized that the observed change in signal signs is not a result of the high intensities because the same sign differences were also observed by Katayama *et al.* in their TAM experiments performed at lower intensities[24]. Additionally, the general mechanisms proposed to qualitatively describe the kinetics are well established and commonly invoked in ultrafast spectroscopy. A more quantitative description of the extraordinary spatial dependence of the decay behaviors observed in the TA kinetics shown in Fig. 3 is obtained through a least squares deconvolution fitting algorithm with explicit consideration of the finite instrumental response; the fit results are given in the Supplementary Table 1.

To explore the possible origins of the different TA signal signs, i.e., positive-signed induced transmission versus negative-signed induced absorption, that were observed across the images of both the pristine $CH_3NH_3PbI_3$ and $CH_3NH_3PbI_3$/PCBM samples, we further examine the decay behavior of those kinetics obtained at the most distinct and visually homogeneous spatial locations of the TA images (e.g., positions 1 and 2 shown in Fig. 2). Because of the presence of nonlinear excited-state relaxation processes in the polycrystalline $CH_3NH_3PbI_3$ films described above, we are able to explicitly consider the following high intensity phenomena: exciton-exciton annihilation[26] and Auger recombination of charged carriers[27, 28]. According to the

analysis described in detail in refs. 29 and 30, the equations describing these nonlinear dynamical processes are:

$$\frac{1}{n_{ex}(t)} - 1 = \gamma_{ex} t \qquad (1)$$

$$\frac{1}{[n_{eh}(t)]^2} - 1 = \gamma_A t \qquad (2)$$

where $n_{ex}(t)$ and $n_{eh}(t)$ in equation (1) and (2) are the populations of excitons and charge carriers at a time delay, *t*, and γ_{ex} and γ_{eh} are the rate constants of exciton-exciton annihilation and Auger recombination, respectively. Note these equations hold only for early delay times when the nonlinear dynamical processes dominate the linear relaxation. As the TA signal, $\Delta A(t)$, is proportional to $n_{ex}(t)$ or $n_{eh}(t)$ depending on the nature of photoexcited species being either excitons or free charge carriers, these equations offer a straightforward means to distinguish the contributing species by simply plotting either an inverse of the TA signal amplitude, $1/\Delta A(t)$, or its square, $1/[\Delta A(t)]^2$, as a function of the delay time, *t*. A linear relationship between the inverse of the TA signal amplitude and delay time is expected if the contributing species are excitons. For free charge carriers, a squared inverse of the TA signal amplitude should instead scale linearly with delay time.

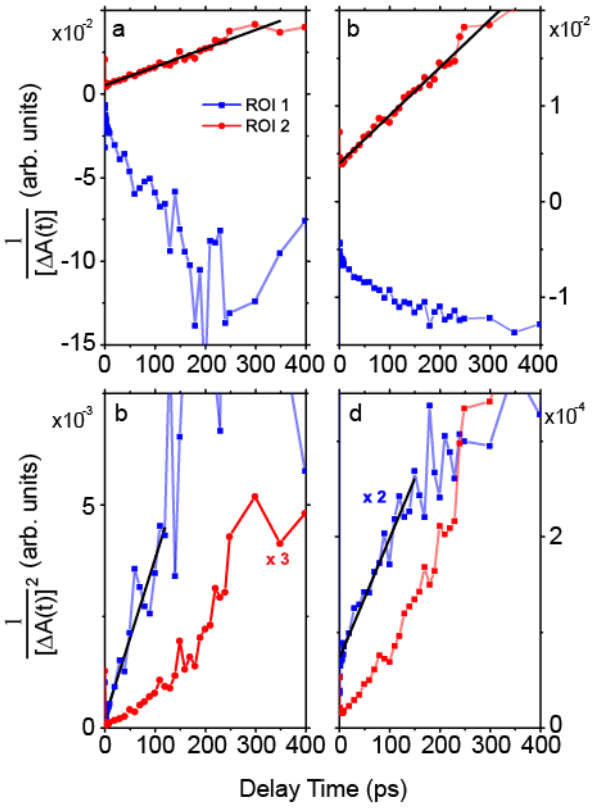

Figure 4. Plot of $1/\Delta A(t)$ and $1/[\Delta A(t)]^2$ vs delay time for the data obtained at position 1 (blue curves) and 2 (red curves) of the pristine $CH_3NH_3PbI_3$ (a, c) and $CH_3NH_3PbI_3$/PCBM (b, d) samples, respectively, as described in the text. The black solid lines are the fits to the linear regions of the corresponding plots, and the fitting parameters are summarized in Supplementary Table 3.

As shown in Fig. 4a and 4b, a linear dependence of $1/\Delta A(t)$ on *t* is clearly evident for the data collected at position 2 of both samples, whereas the results obtained from position 1 obviously deviate from linearity. The linear dependence suggests that the photoexcited species at position 2 in Fig. 2a and 2b are excitons. In comparison, plotting $1/[\Delta A(t)]^2$ for the data acquired at position 1 of both samples shows a linear dependence on *t* in the initial delay time, while such a linearity is not seen for the results obtained at position 2 (see Fig. 4c and 4d). This indicates that

the contributing species at position 1 are free charge carriers. This analysis indicates that both neutral excitons and charge carriers coexist in the polycrystalline perovskite films but they are generated at spatially distinct positions in the sample. Such an analysis is not possible without using high pump and probe pulse intensities with correspondingly high spatial and temporal resolution. The same analysis was also carried out for the data acquired from the $CH_3NH_3PbI_3$/Spiro-OMeTAD sample, but no spatial signature of preferential generation of excitons or charge carriers was ever found, implying that they might not be generated in spatially distinct regions, or, in another word, a mixture of these photoexcited species may coexist at any spatial location in this composite sample. Repeated experiments on a given material (different locations of the same sample or different sample of the same type) always showed the same general transient behaviors and size/length scales of spatial features, indicating repeatability. It is worth noting that the coexistence of excitons and free charge carriers was previously speculated by Katayama *et al.* in explaining their observed spatially dependent TA kinetics in a $CH_3NH_3PbI_3$ based solar cell fabricated on a mesoporous TiO_2 layer[24]. However, no evidence was provided to support this idea, perhaps due to the relatively poor signal-to-noise ratio of their kinetic data, which would limit such an analysis. Thus, our results provide more convincing experimental evidence that excitons and carriers coexist in perovskite thin films, and are generated in distinct spatial domains on the order of several micrometers. It should be pointed out that we exclude exciton-charge interaction and possible contribution from non-germinate free charge carrier recombination that can also lead to a second-order behavior as exciton-exciton annihilation in the above analysis. The reason is that the former is less favorable due to the repulsion force between the same charged carriers and the latter cannot explain the distinct TA signal sign.

The nature of the photoexcited species in perovskite-based materials remains as a pressing open question[1, 31]. This arises from the diverse values of the reported exciton binding energies for three-dimensional $CH_3NH_3PbI_3$ or its mixed halide analogue $CH_3NH_3PbI_{3-x}Cl_x$ crystals, which differ in a range of several tens of meV[4, 5, 10, 32-36] to as small as 2 meV[37], implying either coexistence of excitons and charge carriers or exclusively charge carriers at room temperature, respectively. This lack of unambiguous identification of photoexcited species further leads to controversial assignment regarding the origin of time-resolved PL to either radiative decay of bound electron and hole pairs, i.e., excitons[5] , or radiative recombination of free charge carriers[8]. The coexistence of excitons and charge carriers in polycrystalline perovskite films under high excitation intensities revealed by our TAM results offers more convincing experimental evidence for this unsettled fundamental question. Our finding is in accordance with the predication of Stranks *et al.* based on an analytical model describing both equilibrium properties of free charge carriers and excitons in the presence of electronic sub-bandgap trap states[38]. Those authors showed that the fractions of excitons will increase at higher excitation densities. It is also consistent with the calculations of D'Innocenzo *et al.* using the Saha equation, which also shows a larger fraction of excitons with increasing photoexcitation density[4]. It is unclear, however, why certain spatial locations are preferable for either excitons or free charge carriers and why no such favorable locations are found in the presence of the hole transport layer. This remains a pressing and open question for future studies of these complex materials.

In conclusion, femtosecond transient absorption microscopy was applied to study ultrafast electronic excited-state dynamics in spatially heterogeneous $CH_3NH_3PbI_3$ perovskite based thin

films. Our most striking finding is that the observed TA kinetics are extremely sensitive to the spatial position probed, manifested by distinct TA signals dominated by either positive induced transmission or negative induced absorption characteristics in combination with different decay signatures. Analysis of the decay behavior of the kinetics acquired from spatially distinct locations enabled us to identify coexistence of excitons and free charge carriers in the perovskite films with and without the electron transport layer. The TA images collected at variable time delays exhibit distinct spatial features that are significantly larger in size than the nominally ~1-4 μm grains but are comparable to those observed from recent one- and two-photon fluorescence imaging data. The remarkable difference between the TA kinetic traces obtained by integrating the entire TA images and distinct sub-images further demonstrates the need for a novel spectroscopic technique with simultaneous spatial and temporal resolution in order to unambiguously determine the excited-state relaxation processes and underlying physical mechanisms in such systems with highly spatial heterogeneity. We thus expect that these and future ultrafast nonlinear imaging studies will provide greater insight into the fundamental electronic processes underlying light harvesting and emitting devices.

EXPERIMENTAL METHODS:

Thin films of pristine methylammonium lead tri-iodide ($CH_3NH_3PbI_3$) and its composite structures with either the commonly used electron acceptor [6,6]-phenyl-C_{61}-butyric acid methyl ester (PCBM) or hole transport layer p-type doped 2'-7,7'-tetrakis(N,N-di-p-methoxyphenylamine)-9,9-spirobifluorene (Spiro-OMeTAD) were prepared on 1 mm thick glass substrates following the procedure described in Supplementary Methods. To avoid sample degradation arising from exposure to air and moisture during experiments, each of these films

was covered with a flat 100 μm thickness microscope glass coverslip and all edges were sealed with UV epoxy in a nitrogen atmosphere. The exact sample geometries are therefore glass/ $CH_3NH_3PbI_3$/glass, glass/$CH_3NH_3PbI_3$/PCBM/glass, and glass/$CH_3NH_3PbI_3$/Spiro-OMeTAD/glass (see Supplementary Fig. 1), referred to as pristine $CH_3NH_3PbI_3$, $CH_3NH_3PbI_3$/PCBM and $CH_3NH_3PbI_3$/Spiro-OMeTAD hereafter. The femtosecond TA imaging microscope is based on a 250 kHz regenerative Ti:Sapphire amplifier (~ 50 fs pulses) in combination with a visible optical parametric amplifier, generating desired pump and probe pulses centered at 500 and 800 nm, respectively. The average power levels were 13.1 μW for the pump and 7.0 μW for the probe measured at the sample position, corresponding to pulse energies of 52 pJ and 28 pJ, respectively. The $1/e^2$ radii were estimated to be 407 and 650 nm for the pump and probe beams, and the corresponding fluences were ≈10 and ≈2.1 mJ/cm^2, respectively. These power levels were at the limit of our detection capabilities using an 800 nm probe pulse due to the low TA signal, and thus no pump fluence dependence was measured. Transmission and brightfield images of the same sample area chosen for TAM data acquisition were collected before and after the TAM measurements to ensure no sample damage. A detailed description of this imaging apparatus and the sample characterization/preparation methods is provided in the Supplementary Methods.

ACKNOWLEDGEMENT

Work by M.J.S., B.D. and Y.-Z. M. was supported by the U.S. Department of Energy, Office of Science, Basic Energy Sciences, Chemical Sciences, Geosciences, and Biosciences Division. Perovskite sample preparation by B.Y. and K.X. was conducted at the Center for Nanophase Materials Sciences (CNMS), which is a DOE Office of Science User Facility.

ASSOCIATED CONTENT

Supporting Information:

Description of the material and methods; supplementary tables summarizing the time constants and relative amplitudes of the TA kinetics, the signal amplitudes of the TAM images shown in Figure 2, and the results of the linear fits shown in Figure 4, respectively; supplementary figures showing the sample geometries, the TA kinetics shown in Figure 3 plotted on the entire range of delay time, and a brightfield image acquired after TAM measurements. This material is available free of charge via the Internet at http://pubs.acs.org.

AUTHOR INFORMATION

Corresponding Author

*Email: may1@ornl.gov.

Notes

The authors declare no competing financial interest.

REFERENCES

1. Sum, T. C.; Mathews, N. Advancements in Perovskite Solar Cells: Photophysics Behind the Photovoltaics. *Energy Environ. Sci.* **2014**, *7*, 2518–2534.

2. Zhou, H.; Chen, Q.; Li, G.; Luo, S.; Song, T.-b.; Duan, H.-S.; Hong, Z.; You, J.; Liu, Y.; Yang, Y. Interface Engineering of Highly Efficient Perovskite Solar Cells. *Science* **2014**, *345*, 542-546.

3. Chilvery, A. K.; Batra, A. K.; Yang, B.; Xiao, K.; Guggilla, P.; Aggarwal, M. D.; Surabhi, R.; Lal, R. B.; Currie, J. R.; Penn, B. G. Perovskites: Transforming Photovoltaics, a Mini-Review. *Journal of Photonics for Energy* **2015**, *5*, 057402.

4. D'Innocenzo, V.; Grancini, G.; Alcocer, M. J. P.; Kandada, A. R. S.; Stranks, S. D.; Lee, M. M.; Lanzani, G.; Snaith, H. J.; Petrozza, A. Excitons Versus Free Charges in Organo-Lead Tri-Halide Perovskites. *Nat. Commun.* **2014**, *5*, 3586.

5. Savenije, T. J.; Ponseca, C. S.; Kunneman, L.; Abdellah, M.; Zheng, K. B.; Tian, Y. X.; Zhu, Q. S.; Canton, S. E.; Scheblykin, I. G.; Pullerits, T.; Yartsev, A.; Sundström, V. Thermally Activated Exciton Dissociation and Recombination Control the Carrier Dynamics in Organometal Halide Perovskite. *J. Phys. Chem. Lett.* **2014**, *5*, 2189-2194

6. Hsu, H.-Y.; Wang, C.-Y.; Fathi, A.; Shiu, J.-W.; Chung, C.-C.; Shen, P.-S.; Guo, T.-F.; Chen, P.; Lee, Y.-P.; Diau, E. W. G. Femtosecond Excitonic Relaxation Dynamics of Perovskite on Mesoporous Films of Al_2O_3 and NiO Nanoparticles. *Angew. Chem. Int. Ed.* **2014**, *53*, 9339-9342.

7. Roiati, V.; Colella, S.; Lerario, G.; De Marco, L.; Rizzo, A.; Listorti, A.; Gigli, G. Investigating Charge Dynamics in Halide Perovskite-Sensitized Mesostructured Solar Cells. *Energy Environ. Sci.* **2014**, *7*, 1889-1894.

8. Deschler, F.; Price, M.; Pathak, S.; Klintberg, L. E.; Jarausch, D.-D.; Higler, R.; Hüttner, S.; Leijtens, T.; Stranks, S. D.; Snaith, H. J.; Atatüre, M.; Phillips, R. T.; Friend, R. H. High Photoluminescence Efficiency and Optically Pumped Lasing in Solution-Processes Mixed Halide Perovskite Semiconductors. *J. Phys. Chem. Lett.* **2014**, *5*, 1421-1426.

9. Xing, G. C.; Mathews, N.; Sun, S. Y.; Lim, S. S.; Lam, Y. M.; Grätzel, M.; Mhaisalkar, S.; Sum, T. C. Long-Range Balanced Electron- and Hole-Transport Lengths in Organic-Inorganic $CH_3NH_3PbI_3$. *Science* **2013**, *342*, 344-347.

10. Wu, K.; Bera, A.; Ma, C.; Du, Y.; Yang, Y.; Li, L.; Wu, T. Temperature-Dependent Excitonic Photoluminescence of Hybrid Organometal Halide Perovskite Films. *Phys.Chem.Chem.Phys.* **2014**, *16*, 22476--22481.

11. Shen, Q.; Ogomi, Y.; Chang, J.; Tsukamoto, S.; Kukihara, K.; Oshima, T.; Osada, N.; Yoshino, K.; Katayama, K.; Toyoda, T.; Hayase, S. Charge Transfer and Recombination at the Metal Oxide/$CH_3NH_3PbClI_2$/Spiro-Ometad Interfaces: Uncovering the Detailed Mechanism Behind High Efficiency Solar Cells. *Phys. Chem. Chem. Phys.* **2014**, *16*, 19984-19992

12. Marchioro, A.; Teuscher, J.; Friedrich, D.; Kunst, M.; van de Krol, R.; Moehl, T.; Grätzel, M.; Moser, J.-E. Unravelling the Mechanism of Photoinduced Charge Transfer Processes in Lead Iodide Perovskite Solar Cells. *Nat. Photon.* **2014**, *8*, 250-255.

13. Kim, H.-S.; Lee, C.-R.; Im, J.-H.; Lee, K.-B.; Moehl, T.; Marchioro, A.; Moon, S.-J.; Humphry-Baker, R.; Yum, J.-H.; Moser, J. E.; Grätzel, M.; Park, N.-G. Lead Lodide Perovskite Sensitized All-Solid-State Submicron Thin Film Mesoscopic Solar Cell with Efficiency Exceeding 9%. *Sc. Rep.* **2012**, *2*, 591.

14. Wang, L. L.; McCleese, C.; Kovalsky, A.; Zhao, Y. X.; Burda, C. Femtosecond Time-Resolved Transient Absorption Spectroscopy of $Ch_3nh_3pbi_3$ Perovskite Films: Evidence for Passivation Effect of PbI_2. *J. Am. Chem. Soc.* **2014**, *136*, 12205-12208

15. Manser, J. S.; Kamat, P. V. Band Filling with Free Charge Carriers in Organometal Halide Perovskites. *Nature Photon.* **2014**, *8*, 737-743.

16. Ponseca, J., C. S.; Savenije, T. J.; Abdellah, M.; Zheng, K. B.; Yartsev, A.; Pascher, T.; Harlang, T.; Chabera, P.; Pullerits, T.; Stepanov, A.; Wolf, J.-P.; Sundström, V. Organometal Halide Perovskite Solar Cell Materials Rationalized: Ultrafast Charge Generation, High and Microsecond-Long Balanced Mobilities, and Slow Recombination. *J. Am. Chem. Soc.* **2014**, *136*, 5189-5192.

17. Wehrenfennig, C.; Liu, M. Z.; Snaith, H. J.; Johnston, M. B.; Herz, L. M. Charge-Carrier Dynamics in Vapour-Deposited Films of the Organolead Halide Perovskite $CH_3NH_3PbI_{3-X}Cl_x$. *Energy Environ. Sci.* **2014**, *7*, 2269-2275.

18. Wehrenfennig, C.; Eperon, G. E.; Johnston, M. B.; Snaith, H. J.; Herz, L. M. High Charge Carrier Mobilities and Lifetimes in Organolead Trihalide Perovskites. *Adv. Mater.* **2014**, *26*, 1584-1589.

19. Oga, H.; Saeki, A.; Ogomi, Y.; Hayase, S.; Seki, S. Improved Understanding of the Electronic and Energetic Landscapes of Perovskite Solar Cells: High Local Charge Carrier Mobility, Reduced Recombination, and Extremely Shallow Traps. *J. Am. Chem. Soc.* **2014**, *136*, 13818-13825

20. Xiao, M.; Huang, F.; Huang, W.; Dkhissi, Y.; Zhu, Y.; Etheridge, J.; Gray-Weale, A.; Bach, U.; Cheng, Y.-B.; Spiccia, L. A Fast Deposition-Crystallization Procedure for Highly Efficient Lead Iodide Perovskite Thin-Film Solar Cells. *Angew. Chem. Int. Ed.* **2014**, *53*, 9898-9903.

21. Nie, W.; Tsai, H.; Asadpour, R.; Blancon, J.-C.; Neukirch, A. J.; Gupta, G.; Crochet, J. J.; Chhowalla, M.; Tretiak, S.; Alam, M. A.; Wang, H.-L.; Mohite, A. D. High-Efficiency Solution-Processed Perovskite Solar Cells with Millimeter-Scale Grains. *Science* **2015**, *347*, 522-525.

22. Min, W.; Freudiger, C. W.; Lu, S.; Xie, X. S. Coherent Nonlinear Optical Imaging: Beyond Fluorescence Microscopy. *Annu. Rev. Phys. Chem.* **2011**, *62*, 507-530.

23. Wen, X. M.; Sheng, R.; Ho-Baillie, A. W. Y.; Benda, A.; Woo, S.; Ma, Q. S.; Huang, S. J.; Green, M. A. Morphology and Carrier Extraction Study of Organic-Inorganic Metal Halide Perovskite by One- and Two-Photon Fluorescence Microscopy. *J. Phys. Chem. Lett.* **2014**, *5*, 3849-3853

24. Katayama, T.; Jinno, A.; Takeuchi, E.; Ito, S.; Endo, M.; Wakamiya, A.; Murata, Y.; Ogomi, Y.; Hayase, S.; Miyasaka, H. Inhomogeneous Deactivation with UV Excitation in Submicron Grains of Lead Iodide Perovskite-Based Solar Cell as Revealed by Femtosecond Transient Absorption Microscopy. *Chem. Lett.* **2014**, *43*, 1656-1658

25. Sheng, C. X.; Zhang, C.; Zhai, Y.; Mielczarek, K.; Wang, W.; Ma, W.; Zakhidov, A.; Vardeny, Z. V. Exciton Versus Free Carrier Photogeneration in Organometal Trihalide Perovskites Probed by Broadband Ultrafast Polarization Memory Dynamics. *Phys. Rev. Lett.* **2015**, *114*, 116601.

26. van Amerongen, H.; Valkunas, L.; van Grondelle, R. *Photosynthetic Excitons*. World Scientific: Singapore, New Jersey, London, Hongkong, 2000.

27. Ghanassi, M.; Schanne-Klein, M. C.; Hache, F.; Ekimov, A. I.; Ricard, D.; Flytzanis, C. Time-Resolved Measurements of Carrier Recombination in Experimental Semiconductor-Doped Glasses: Confirmation of the Role of Auger Recombination. *Appl. Phys. Lett.* **1993**, *62*, 78-80.

28. Klimov, V. I.; Mikhailovsky, A. A.; McBranch, D. W.; Leatherdale, C. A.; Bawendi, M. G. Quantization of Multiparticle Auger Rates in Semiconductor Quantum Dots. *Science* **2000**, *287*, 1011-1013.

29. Htoon, H.; Hollingsworth, J. A.; Dickerson, R.; Klimov, V. I. Effect of Zero- to One-Dimensional Transformation on Multiparticle Auger Recombination in Semiconductor Quantum Rods. *Phys. Rev. Lett.* **2003**, *91*, 227401.

30. Ma, Y.-Z.; Valkunas, L.; Bachilo, S. M.; Fleming, G. R. Exciton Binding Energy in Semiconducting Single-Walled Carbon Nanotubes. *J. Phys. Chem. B* **2005**, *109*, 15671-15674.

31. Stranks, S. D.; Eperon, G. E.; Grancini, G.; Menelaou, C.; Alcocer, M. J. P.; Leijtens, T.; Herz, L. M.; Petrozza, A.; Snaith, H. J. Electron-Hole Diffusion Lengths Exceeding 1 Micrometer in an Organometal Trihalide Perovskite Absorber. *Science* **2013**, *342*, 341-344

32. Ishihara, T. Optical Properties of PbI-Based Perovskite Structures. *J. Lumin.* **1994**, *60&61*, 269-274.

33. Sun, S. Y.; Salim, T.; Mathews, N.; Dyuchamp, M.; Boothroyd, C.; Xing, G. C.; Sum, T. C.; Lam, Y. M. The Origin of High Efficiency in Low-Temperature Solution-Processable Bilayer Organometal Halide Hybrid Solar Cells. *Energy Environ. Sci.* **2014**, *7*, 399-407.

34. Hirasawa, M.; Ishihara, T.; Goto, T.; Uchida, K.; Miura, N. Magnetoabsorption of the Lowest Exciton in Perovskite-Type Compound $(CH_3NH_3)PbI_3$. *Physica B* **1994**, *201*, 427-430.

35. Koutselasy, I. B.; Ducassez, L.; Papavassiliou, G. C. Electronic Properties of Three- and Low-Dimensional Semiconducting Materials with Pb Halide and Sn Halide Units. *J. Phys.: Condens. Matter* **1996**, *8*, 1217–1227.

36. Tanaka, K.; Takahashi, T.; Ban, T.; Kondo, T.; Uchida, K.; Miura, N. Comparative Study on the Excitons in Lead-Halide-Based Perovskitetype Crystals $CH_3NH_3PbBr_3$ $CH_3NH_3PbI_3$. *Solid State Commun.* **2003**, *127*, 619-623.

37. Lin, Q.; Armin, A.; Nagiri, R. C. R.; Burn, P. L.; Meredith, P. Electro-Optics of Perovskite Solar Cells. *Nat. Photon.* **2015**, *9*, 106-112.

38. Stranks, S. D.; Burlakov, V. M.; Leijtens, T.; Ball, J. M.; Goriely, A.; Snaith, H. J. Recombination Kinetics in Organic-Inorganic Perovskites: Excitons, Free Charges, and Subgap States. *Phys. Rev. Applied* **2014**, *2*, 034007.